# Three Pulse Photon Echo Peak Shift Study of the B800 Band of the LH2 Complex of *Rps. acidophila* at Room Temperature: A Coupled Master Equation and Nonlinear Optical Response Function Approach

**Ritesh Agarwal, Mino Yang, Qing-Hua Xu, and Graham R. Fleming***

*Department of Chemistry, University of California at Berkeley, and Physical Biosciences Division, Lawrence Berkeley National Laboratory, Berkeley, California 94720*

*Received: August 29, 2000; In Final Form: December 6, 2000*

Three pulse photon echo peak shift (3PEPS) data were obtained for the B800 band of *Rps. acidophila* (strain 10050) at room temperature. The peak shift decays on two time scales: a sub 100 fs decay owing to the ultrafast solvation by the protein bath and a 500−600 fs decay to a value of 2.5 fs at 1.2 ps. Here we present a novel method that properly incorporates the effect of energy transfer on the nonlinear response functions to simulate the peak shift for weakly coupled, multi-chromophoric energy transfer systems. The method involves calculation of third-order response functions for energy transfer systems to account for the interaction of the laser pulses with the chromophores, whereas the energy transfer kinetics is incorporated by solving the master equation for the whole ring of B800 pigments. The effect of disorder on spectral overlaps is taken into account by a Monte Carlo sampling procedure that selects transition frequencies from a Gaussian distribution of site energies. The peak shift is then calculated by combining ensemble-averaged population kinetics with the appropriate response functions. We estimate the energy transfer time within the B800 band to be ∼500−600 fs, and the experiments are well described by Forster theory level calculations including energy disorder. By simultaneously modeling the peak shift data and the linear absorption spectrum, we suggest the presence of two levels of disorder (i.e., partially correlated disorder) in the B800 band. Strong beats are also found in our data with a frequency of 165 $cm^{-1}$.

## 1. Introduction

The primary processes of photosynthesis involve the capture of sunlight and efficient transfer of the resulting excitation energy to the reaction center where a series of electron transfer reactions create a transmembrane potential which is used to drive chemical reactions.[1] The process of capture of solar photons and transfer of this excitation energy to the reaction center is achieved by a network of pigment−protein complexes called light-harvesting complexes. In many photosynthetic purple bacteria, the light-harvesting antenna consists of a core antenna (which is found to encircle the reaction center) called the LH1, which absorbs around 875 nm, and peripheral antenna, LH2, with major absorption around 800 and 850 nm (called the B800 and B850 bands, respectively). The energy is first transferred within the light-harvesting complex and then transferred to the reaction center. The antenna complexes thus enable the reaction centers to operate much more efficiently by collecting light from a broader spectral range.

Recently the crystal structure of the LH2 complex of *Rhodopseudomonas acidophila* was solved to a resolution of 2.5 Å,[2] which led to intense study of the photophysical processes in these complexes. The complex has 9-fold circular symmetry (while that of *Rhodospirillum molichianum* has 8-fold symmetry),[3] and the basic unit is comprised of α- and β-apoprotein, three bacteriochlorophylls (BChl), and at least one carotenoid. The three-dimensional structure shows that the B800 ring is comprised of 9 bacteriochlorophyll (BChl) molecules whereas B850 forms a circular aggregate of 18 closely spaced BChl molecules. The Mg−Mg distance between the BChl's in B800 ring is 21 Å, while the Mg−Mg distance between the BChl's in B850 within the α-subunit is 8.7 Å and between adjacent units is 9.7 Å.

The energy transfer dynamics within LH2 can be broken down into three processes: B800−B800 transfer, B800−B850 transfer, and B850−B850 transfer.[4−6] All three processes have been the subject of extensive study.[4−6] The B800−B850 process is the best characterized and occurs on a 650−900 fs time scale at room temperature, slowing to 2 ps at low temperature.[7−15] Scholes and Fleming recently presented a theoretical description of B800−B850 energy transfer based on extension of Forster theory to include both disorder and an excitonic manifold of acceptor states.[16] Their treatment seems to capture the essentials of the process and emphasizes the increase in the spectral cross section of the acceptor states owing to strong excitonic interactions and the presence of disorder. Energy transfer processes within the more strongly coupled B850 molecules[17,18] continue to generate considerable debate on issues such as the degree of localization and the mechanism of transport.[6,11,19−25] Whatever the details of the mechanism, it seems clear that a sophisticated theoretical model such as multilevel Redfield theory[26] is required to relate the experimental observations to the miscroscopic dynamics.

In principle, the situation for B800−B800 energy transfer should be much simpler. The electronic coupling between the pigments in the B800 band is estimated to be ∼30 $cm^{-1}$.[17,18] We expect this value is low enough with respect to the homogeneous and inhomogeneous spectral widths to allow a description of the energy transfer as hopping between localized molecular states via Forster theory.[27] This process should then allow a detailed examination of the ability of simple models to characterize energy transfer in an inhomogeneous system. However, energy transfer within the B800 band of LH2 has been difficult to characterize unambiguously, in large measure because the competitive B800−B850 transfer removes the B800

10.1021/jp0031146 CCC: $20.00 
Published on Web 02/10/2001

population on a subpicosecond time scale and thus limits the time window of most experiments.[8,9,12,13,28,30−32]

During our exploration of the three pulse photon echo peak shift (3PEPS) method,[21,33−39] we have found that this technique has a remarkable insensitivity to processes taking population out of the laser bandwidth, which we refer to as interband transfer, while having high sensitivity to intraband transfer in a spectrally inhomogeneous system. To exploit this advantage, it was necessary to develop a method for calculating the nonlinear optical signal that incorporated a detailed model of the energy transfer dynamics, including reversible energy transfer and distributions of rates based on site energy distributions and (if such information was available) distributions of coupling matrix elements. In ref 44, Yang and Fleming described such an approach based on factoring the nonlinear optical phase factors and population dynamics and explored the validity of such an approximation. Such a factorization neglects the effect of site energy correlation induced by the energy transfer itself and has been shown to be a good approximation in a weakly coupled system if the inhomogeneous population kinetics results largely from diagonal (i.e,. energy) disorder and the laser spectrum is broad enough to cover the entire donor spectrum. Also, the effect of energy transfer induced correlation is not significant if the thermal energy fluctuation of the site energies is comparable to the inhomogeneous width.

With such a model in place it becomes possible to explicitly calculate the population of the molecules acting as intermediates between the optically interrogated donors and acceptors, via a master equation method.[40] This approach allows us to test the validity of the Forster approach to B800−B800 energy transfer, to extract the mean time scale of the transfer, and to explore in detail the nature of the energetic disorder in this system. In particular we consider whether each LH2 system contains the full amount of disorder or whether correlation in the B800 site energies exists within each individual LH2 complex. Such a correlation has recently been proposed from an analysis of low-temperature single molecule spectra of the B800 band.[41]

## 2. Experimental Section

The B800−850 LH2 complex *Rps. acidophila* strain 10050 samples were generously provided by Professor Cogdell and co-workers. The experiments were performed using a home-built cavity dumped Ti:sapphire laser. The laser cavity was tuned to operate at a central frequency of 800 nm by inserting intracavity apertures. The spectrum was tuned such that there was minimum excitation of the B850 band pigments. The pulses generated were ∼25 fs (fwhm) at a repetition rate of 250 kHz. The average pulse energy at the sample was approximately 1 nJ per pulse. The sample was flowed through a 100 mm path length quartz cell by a peristaltic pump. The optical density of the sample was 0.15 at 800 nm for a 100 mm cell. Before measuring on the biological sample, peak shift data were collected on laser dyes dissolved in liquids to ensure that the long-time peak shift was zero (<1 fs).[42] This procedure ensures a good alignment of the interoferometer.

The three pulse photon echo peak shift measurements were carried out as previously described.[33] In short, three laser beams (of roughly equal intensities and parallel polarization) were arranged in equilateral triangle geometry and focused on the sample. Changing the polarization of the third pulse from parallel to perpendicular does not change the peak shift decay behavior significantly.[43] The first pulse interacts with the sample to create an optical coherence, the second pulse creates a population state, in either the ground or excited state, and the third pulse creates a coherence state again. If the phase of the second coherence state is opposite that of the first coherence, an echo signal is generated. The time-integrated echo profiles were simultaneously measured in the two phase-matched directions, $\mathbf{k} = \mathbf{k}_3 \pm (\mathbf{k}_1 - \mathbf{k}_2)$, as a function of the coherence period, $\tau$, for fixed values of the population period, $T$. The echo peak shifts ($\tau^*(T)$) obtained from the position where the integrated echo profiles peak in intensity were recorded as a function of population period ($T$).

## 3. Theoretical Model for the Peak Shift

Yang and Fleming extended the theory for 3PEPS to model weakly electronically coupled systems coupled to a harmonic bath.[38,44] This theory properly incorporates the effect of energy transfer on nonlinear response functions. It has been described in detail previously, and we present the salient features of the theory for completeness.[39,40,43] The system is modeled as a collection of donors and acceptors associated with the *intraband* energy transfer which can also undergo interband energy transfer processes on each site. The dynamic fluctuations induced by the bath at each site are assumed to be the same and are described by a transition frequency correlation function, $M(t)$. The $M(t)$ is in general a complex function for a quantum mechanical system. However, in the high-temperature limit, the real and the imaginary part of the $M(t)$ are assumed to be the same (they become identical at infinite temperature). The $M(t)$ at high temperatures is given by

$$\mathrm{Re}\{M(t)\} \approx \mathrm{Im}\{M(t)\} \approx \mathrm{Re}\{\langle \delta\Delta E(t)\, \delta\Delta E(0)\rangle / \langle \delta^2 \Delta E(0)\rangle\} \quad (1)$$

where $\delta\Delta E$ is the Heisenberg operator of the fluctuating energy difference between the ground and excited states.[35] The dynamic fluctuations at different sites (donor and acceptor) are however assumed to be completely uncorrelated in our model. Energy transfer within (intraband) and outside (interband) the laser spectrum is incorporated by introducing new pathways which contribute to the third-order nonlinear polarization.

Figure 1 gives a simplified picture of the model used for energy transfer systems in terms of double-sided Feynman diagrams. Two main contributions to the response functions were described: the first term arises when the three pulses interact with the donor while the excitation remains on the donor. The signal has rephasing capability and hence produces an echo. The second term describes the dynamics of the excitation after it has migrated to the acceptor and is due to the interaction of the first two pulses with the donor and the third interaction with the acceptor after the energy transfer. This has no rephasing capability for uncorrelated fluctuations and hence gives a free induction decay (FID) signal. The peak shift, which measures the rephasing capability of the nonlinear polarization, decreases as the relative contribution of the FID to the total signal increases. The effect of interband energy transfer on peak shift data is slightly different. Due to the removal of the population out of the laser spectral window, the third pulse cannot interact with it and hence it does not lead to a decay of peak shift. Instead, it leads to a decay of the signal intensity. Although the interband energy transfer can affect the peak shift behavior in the nonimpulsive limit, its effect is subtle[38,39] and we emphasize that the FID signal resulting in decay of the peak shift is generated by only the *intraband* energy transfer process.

The nonlinear optical response function associated with the energy transfer system is written as

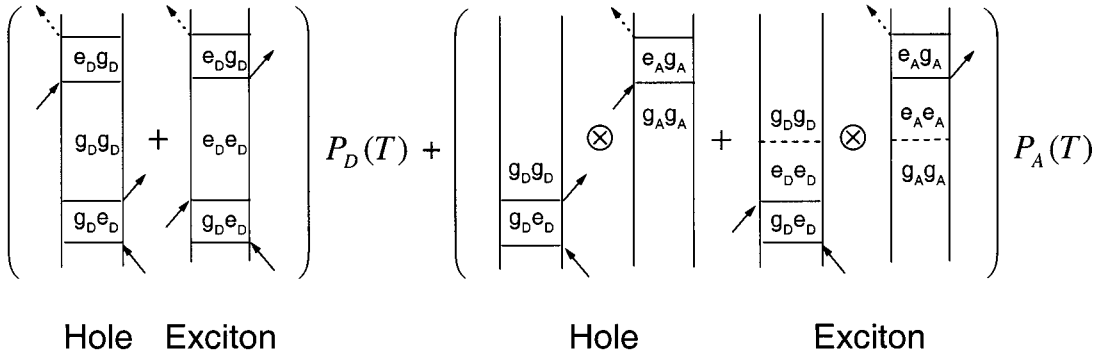


**Figure 1.** Model used to simulate the peak shift for energy transfer systems within the weak coupling limit. Double-sided Feynman diagrams are shown for echo-generating term (first diagram) and for free induction decay like signal (second diagram).[38] The arrows indicate the interaction of the donor or acceptor with the incoming fields. "g" and "e" indicate ground and excited state, respectively, whereas "D" and "A" stand for donor and acceptor.

$$R(t,T,\tau;\Gamma) = R_{\text{echo}}(t,T,\tau;\Gamma)\, P_{\text{D}}(T;\Gamma) + R_{\text{FID}}(t,\tau;\Gamma)\, P_{\text{A}}(T;\Gamma) \tag{2}$$

where $\Gamma$ denotes a set of static variables affecting the optical response. The first term is the response function for the donor, which generates an echo signal similar to a two-level system coupled to the bath. The second term of eq 2 is the third-order response function for the pathway where the first two interactions are with the donor molecule and the third interaction is with the acceptor whose site energy fluctuations are completely uncorrelated with the donor.[38] This term produces a free induction decay signal. $P_{\text{D}}(T)$ and $P_{\text{A}}(T)$ are the donor and acceptor populations, respectively. In the presence of inhomogeneity, eq 2 should be averaged over a distribution of the static variables $\Gamma$:

$$R(t,T,\tau) = \langle R(t,T,\tau;\Gamma)\rangle_\Gamma \approx \langle R_{\text{echo}}\rangle_\Gamma \langle P_{\text{D}}\rangle_\Gamma + \langle R_{\text{FID}}\rangle_\Gamma \langle P_{\text{A}}\rangle_\Gamma \tag{3}$$

The factorization shown in eq 3 was discussed in ref 44 and introduces little error in a weakly coupled system, provided the laser bandwidth is broad enough to cover the entire spectrum on the donor molecules. This separation of the phase factors responsible for the nonlinear optical signals and the population kinetics allows for modeling of much more complex energy transfer systems than have been considered previously, since now the population dynamics of the intermediate molecules can be explicilty calculated via a master equation method.[40] The strategy used to calculate the signal is shown in Figure 2. The third-order optical response functions for a donor−acceptor pair are used to account for the interaction of the chromophores with the laser pulses whereas energy transfer kinetics is incorporated by solving the master equation for the whole ring of weakly coupled B800 chromophores. The initial excitation is placed on one chromophore in a ring (randomly selected), and that chromophore serves as a donor molecule with the other chromophores in the ring being acceptor molecules. The energy transfer mechanism was modeled using Forster theory, i.e., incoherent hopping of excitation energy. The time dependent occupation probabilities of each chromophore in the ring were calculated by solving nine coupled differential equations using the Pauli master equation

$$\frac{\mathrm{d}P_i(t)}{\mathrm{d}t} = \sum_{j=1}^{9} F_{ij}P_j(t) - \sum_{j=1}^{9}\left(F_{ji} + \frac{1}{\tau_i}\right)P_i(t) \tag{4}$$

where $F_{ij}$ is the rate constant for transfer from site $j$ to $i$ and $P_i(t)$ is the time-dependent probability of finding the excitation

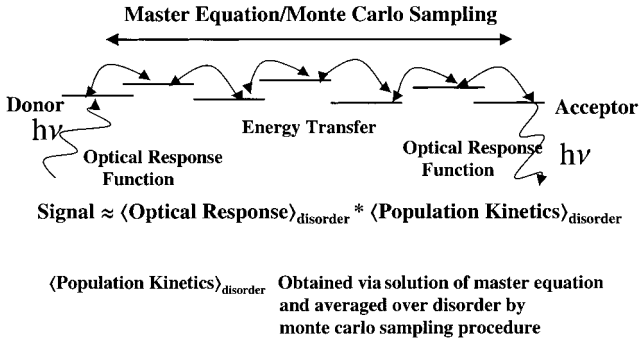


**Figure 2.** Schematic diagram of the method used to calculate the peak shift for spectrally disordered, weakly coupled energy transfer systems. Field−matter interactions are accounted for by third-order response functions for weakly coupled systems. Energy transfer is modeled by a solution of the master equation for the electronically coupled pigments, and a Monte Carlo sampling procedure accounts for the spectral disorder.

on the $i$th site. $\tau_i$ is the lifetime of the excited state (which in this case corresponds to B800−B850 energy transfer time). The downhill rate constants are calculated from the overlap of the donor emission spectrum and the acceptor absorption spectrum. The uphill transfer rates are calculated via the detailed balanced equation

$$F_{ji} = F_{ij}\exp(-\Delta E_{ij}/kT) \tag{5}$$

where $\Delta E_{ij}$ is the difference between the peak frequencies of the two absorption bands (donor and acceptor).

The Pauli master equation is solved using a Green function solution of the coupled equations.[40] Each chromophore in the ring is assigned a specific site energy that is randomly chosen from a Gaussian distribution of disorder values by a Monte Carlo sampling procedure. Hence the effect of disorder on energy transfer is taken into account by calculating spectral overlaps via homogeneous line shapes centered at a site energy that is randomly chosen. The acceptor population kinetics is obtained by summing the populations of all but the donor chromophore in the ring. The ensemble averaged population kinetics is then obtained by averaging over 3000 rings to ensure convergence. The resulting donor ($P_{\text{D}}(T)$) and acceptor ($P_{\text{A}}(T)$) populations are then combined with the response functions (eq 3) associated with the echo and free induction decay respectively to calculate the peak shift. In our model, the dynamic fluctuations of the individual chromophores are assumed to be completely uncorrelated, and thus the memory of dynamic fluctuations is completely lost due to energy transfer. Hence the population

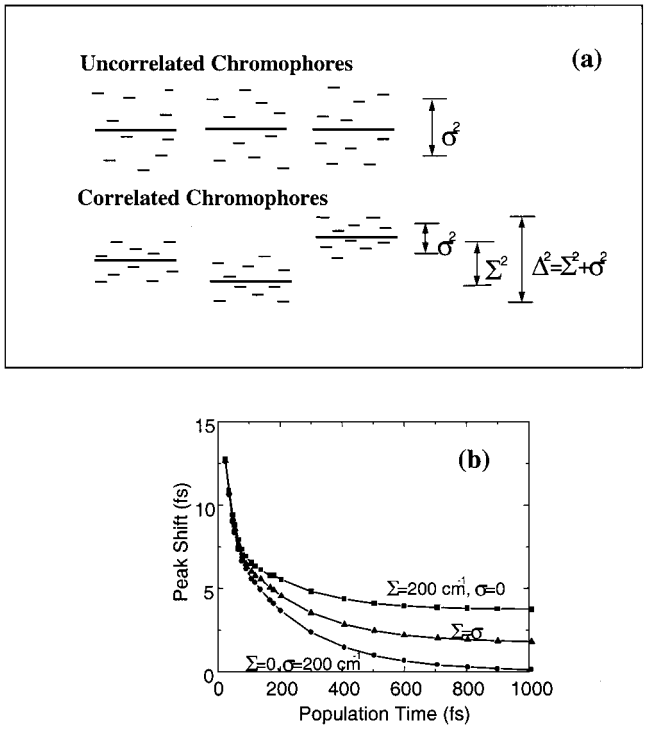


**Figure 3.** (a) Schematic diagram illustrating uncorrelated disorder ($\sigma \neq 0$, $\Sigma = 0$) and two levels of disorder (partially correlated chromophores; $\sigma$, $\Sigma \neq 0$) used in our calculations. (b) Model calculation of the peak shift for different values of $\sigma$ and $\Sigma$. The energy transfer time is 300 fs, and the total inhomogeneous width is fixed at 200 cm$^{-1}$. The solid dots are for $\sigma = 200$ cm$^{-1}$, $\Sigma = 0$; the triangles are for $\sigma = \Sigma = 141$ cm$^{-1}$; and the squares are for $\sigma = 0$, $\Sigma = 200$ cm$^{-1}$. The presence of a finite value of the peak shift is clearly seen at long-time delays for a nonzero value of $\Sigma$.

that is transferred from the donor to any of the acceptor molecules gives a free induction decay signal and thus leads to a decay of peak shift. Should the excitation return to the initial donor owing to reversible energy transfer, the memory of the dynamic fluctuations is assumed to be completely lost whereas the static correlation memory is completely retained and hence can give rise to an echo signal. These assumptions seem reasonable if the time scale of dynamic fluctuations is fast compared to the time scale of the energy transfer process. In our model, we also take into account the transfer of excitation energy from the B800 pigments to the B850 ring on a time scale of 800 fs.

The above discussion takes into account only the distribution of static energy within a ring of chromophores and assumes that the distribution of static energies is the same for all the rings in an ensemble. However, it is possible that the mean of the distribution of static energy within a ring can be different from other rings; i.e., there can be a distribution of the mean of static energy between different rings, see Figure 3a. In ref 44, Yang and Fleming addressed the effect of two levels of distribution of static disorder in electronically coupled systems on peak shift. They modeled the system as a collection of independent cells, in each of which the chromophores has a Gaussian distribution of static energies given by $\sigma$(standard deviation). The distribution of means of the individual cells is given by $\Sigma$(standard deviation). In other words, this two-level distribution is equivalent to having some degree of correlation in the disorder within a cell; i.e., it allows the chromphores in a cell to assume values within a limited range. The total width of the static disorder, $\Delta$, is given by $(\sigma^2 + \Sigma^2)^{1/2}$. Energy transfer within the chromophores in a cell leads to a similar effect as

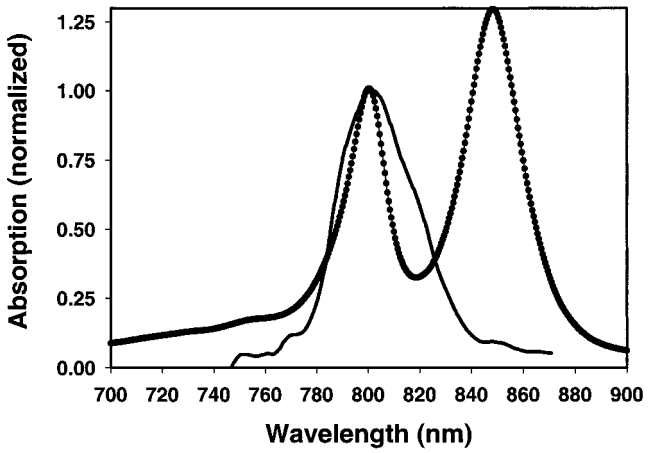


**Figure 4.** Absorption spectrum of the B800−B850 complex of *Rps. acidophila* at room temperature. Also shown is the laser pulse spectrum.

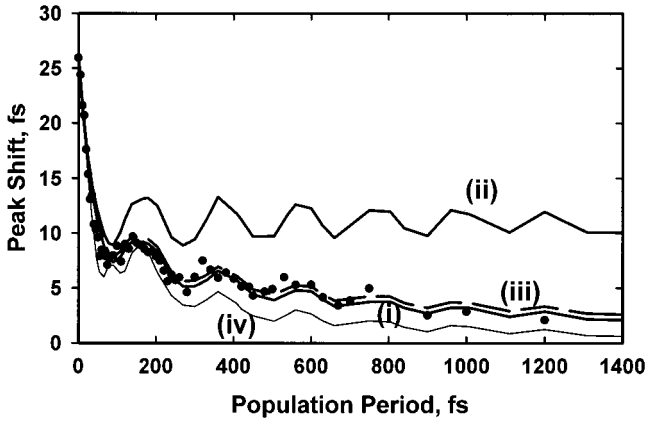


**Figure 5.** 3PEPS data for the B800 band of the LH2 complex of *Rps. acidophila* (filled circles). The solid lines show the simulated peak shift. (i) Simulation with energy transfer within the B800 band. The B800−B850 transfer is also included. $\sigma = 150$ cm$^{-1}$. (ii) Simulation with no B800−B800 transfer (i.e., electronic coupling between the B800 pigments is set to zero). (iii) Simulation with no B800−B850 energy transfer. (iv) Simulation with $\sigma = 100$ cm$^{-1}$ (static disorder width that simulates the absorption spectrum).

discussed above, i.e., it leads to a loss of phase memory due to uncorrelated fluctuations, whereas since the different cells are independent, the memory of static disorder between different cells is retained. Model peak shift calculations for different values of $\sigma$ and $\Sigma$ with an energy transfer time of 300 fs (homogeneous rate constant) are shown in Figure 3b. It can be seen clearly that a nonzero value of $\Sigma$ leads to a finite value of long-time peak shift as the memory of this static distribution is retained for very long times whereas the memory of the static distribution $\sigma$ is lost due to energy transfer.

## 4. Results

The room-temperature absorption spectrum of B800−850 complex of *Rps. acidophila* is shown in Figure 4 along with the pulse spectrum. The peak shift data are shown in Figure 5 (solid circles). The value of the initial peak shift is ∼26 fs and is large compared to the initial peak shift values observed for laser dyes dissolved in polar solvents.[33] Large values of initial peak shift are indicative of weak electron−phonon coupling strength. This is because a weak electron−phonon coupling leads to a small contribution of the homogeneous component to the dephasing and hence a larger value of the initial peak shift. The experimental peak shift decays rapidly on two time

scales; a sub 100 fs decay followed by a 500−600 fs time scale decay to a value of $\tau^* \sim 2.5$ fs at 1.2 ps. Quantum beats of considerable amplitude and with a frequency of 165 $cm^{-1}$ are clearly evident in the peak shift data, which persist up to at least 1 ps. Such beats, to the best of our knowledge, have not been observed in the pump−probe studies on the B800 band.

### 5. Simulation of the Peak Shift Data

We explore two models for our data. First we consider completely uncorrelated disorder ($\Sigma = 0$), and then we consider the case of partly correlated disorder (i.e., $\Sigma$, $\sigma \neq 0$).

**Case 1. $\Sigma = 0$ (Uncorrelated Disorder).** In energy transfer systems, the peak shift simulation contains two components: (a) the bath (or solvation) dynamics, given by the transition frequency correlation function $M(t)$, and (b) energy transfer kinetics. For the LH2 complex, there exists little information on the solvation dynamics of the protein. Hence we resort to the peak shift data available on the B820 subunit of LH1−a similar pigment−protein complex with no energy transfer.[36] The peak shift data on the B820 subunit revealed an ultrafast solvation component and static inhomogeneity. Similarly, the peak shift decay for dilute dye solutions in polymer glasses reveals an ultrafast component and long-time inhomogeneity.[45,46] The diffusive processes in proteins and glasses can be regarded as static on the time scale of our experiments.[46] Based on these observations, we model our $M(t)$ with a Gaussian component and static inhomogeneity. We also included the intramolecular vibrations of the bacteriochlorophyll molecules in $M(t)$. The frequency of the mode that clearly appears as quantum beat was determined to be 165 $cm^{-1}$ with a coupling strength of 65 $cm^{-1}$. The frequencies of high-frequency modes were obtained from hole burning and fluorescence experiments.[47,48] The peak shift decay within the initial 200 fs is due to a combination of the ultrafast Gaussian component and the destructive interference of the high-frequency intramolecular modes. Recent results from our laboratory have indicated that peak shift data (especially for laser dyes dissolved in polar solvents) are sensitive to the excitation wavelengths used in the experiments.[49] This results from the excitation of different vibronic states at different excitation wavelengths. The effect is more pronounced if the excitation wavelength is tuned to the blue side of the absorption spectrum. However, in the case of light-harvesting complexes, the situation is more favorable than dye chromophores dissolved in condensed phase. The reorganization energy for both inter- and intramolecular motions in light-harvesting complexes is extremely small. Therefore, large values of the initial peak shift are observed. For such systems, good agreement between experimental and calculated initial peak shift values is obtained, because the destructive interference of the intramolecular vibrations plays a relatively small role in the initial dynamics. Furthermore, these systems have significant inhomogeneous broadening, and we believe that our analysis will give reasonable values of electron−phonon coupling strengths, inhomogeneity, and energy transfer time scales. Therefore, we model our $M(t)$ with a Gaussian component (coupling strength 110 $cm^{-1}$, time constant 50 fs) along with a few high-frequency modes as given in Table 1. The sub 100 fs portion of the peak shift is described adequately by our $M(t)$.

The energy transfer kinetics was modeled using a microscopic model of the B800 ring with nearest-neighbor electronic coupling of 30 $cm^{-1}$ and next-nearest neighbor coupling of 4 $cm^{-1}$.[17,18] The B800−B850 energy transfer rate was fixed at $(800\ fs)^{-1}$. The homogeneous spectral line shape was calculated from the model $M(t)$ given in Table 1. The Stokes shift obtained from the homogeneous line shape is 100 $cm^{-1}$. Smaller values for the Stokes shift have been reported for light-harvesting complexes, but those experiments were done at very low temperatures.[4,50,51] The B800 band has been shown to be predominantly inhomogeneously broadened by hole burning experiments at low temperatures.[47] Direct evidence of spectral inhomogeneity within the B800 band has recently been obtained from single molecule spectroscopy of the LH2 complex at low temperatures.[41,52−54] In a disordered system such as the B800 band of LH2, the static disorder gives rise to a broad distribution of rates that leads to nonexponential energy transfer kinetics. Since the peak shift is very sensitive to intraband energy transfer, it reflects clearly any nonexponential behavior. The static disorder value that gave the best fit to the data was $\sigma = 150$ $cm^{-1}$ (standard deviation). The simulated peak shift is shown as a solid line in Figure 5, curve (i). Changing the values of static disorder and Stokes shift within reasonable limits (±20%) did not drastically change the peak shift decay. In Figure 5, curve (ii), a peak shift calculation is shown when the electronic coupling between the B800 bacteriochlorophylls is set to zero. Clearly, the 500−600 fs decay component cannot be captured by this calculation.

**TABLE 1: Simulation Parameters for 800 nm Peak Shift Data**[a]

| | coupling strength, $\langle\Delta\omega^2\rangle^{1/2}$, $cm^{-1}$ | $\tau$, fs | $\nu$, $cm^{-1}$ | $\tau_{damping}$, fs | phase, rad |
|---|---|---|---|---|---|
| Gaussian | 110 | 50 | | | |
| vibration | 70 | | 560 | 100 | 0 |
| vibration | 50 | | 432 | 300 | 0 |
| vibration | 65 | | 165 | 1500 | 0 |

[a] $M(t)$ is modeled as a sum of a Gaussian component and damped cosines

$$M(t) = (\langle\Delta\omega_g^2\rangle e^{-(t/\tau_g)^2} + \sum_i \langle\Delta\omega_i^2\rangle \cos(\omega_i t + \phi_i) \exp(-t/\tau_i))/ \sum_k \langle\Delta\omega_k^2\rangle + \Delta_{in}^2$$

where $\langle\Delta\omega^2\rangle$ is the coupling strength for each term, $\tau_i$ are time constants, $\omega_i$ are the frequencies of impulsively excited vibrations, $\phi_i$ are the corresponding phase factors, and $\Delta_{in}$ is the standard deviation of the inhomogeneous width. Parameters for $M(t)$ (solvation correlation function) in the absence of energy transfer are given above.

The ensemble-averaged population kinetics of the donor and acceptor chromophores are shown in Figure 6a. The kinetics is shown for one nearest-neighbor (dashed line) and one next-nearest neighbor chromophore (dash−dot line) along with the sum of the populations of all the acceptors (solid line). It can be seen in Figure 6a that the nearest neighbor of the donor gets significant population prior to energy transfer to the B850 band. We would like to emphasize that it is this complex behavior of the population kinetics that leads to the decay of peak shift. The full model including both nearest and next nearest neighbor interactions can simulate the observed peak shift decay behavior. To illustrate the effect of energy transfer from the B800 to the B850 ring on the peak shift, we show the population kinetics in Figure 6b but now neglecting the B800−B850 energy transfer. The corresponding peak shift calculation is shown in Figure 5, curve (iii). As can be seen, the effect of B800−B850 energy transfer on the peak shift is minor even though the population kinetics look significantly different for the two cases (Figure 6a,b). The energy transfer from B800−B850 changes the relative population of donors and acceptors and therefore does indirectly influence the peak shift, but the effect is small. These calculations strongly suggest that the intermediate time scale decay in the peak shift reflects the B800−B800 transfer.

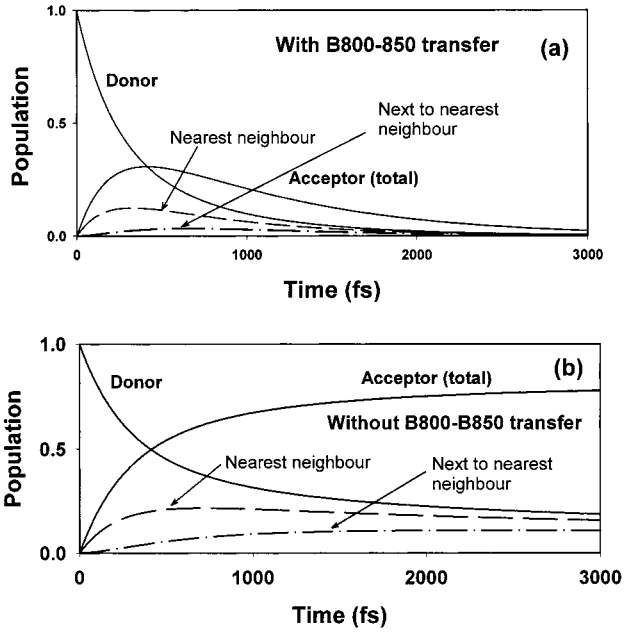


**Figure 6.** Ensemble-averaged population kinetics for the B800 pigments. The donor is the chromophore on which the initial excitation is placed at time $t = 0$. Acceptor (total) is the sum of populations of all the other chromophores in the B800 ring except the donor chromophore. (a) Ensemble-averaged population kinetics with B800−B850 energy transfer set at 800 fs for all the B800 pigments. (b) Ensemble-averaged kinetics with no B800−B850 energy transfer. The donor and acceptor (total) population kinetics is given by solid lines. The dashed line is the population kinetics for the nearest neighbors (of the donor). The dash−dotted line is the population kinetics for the next-nearest neighbors of the donor.

Since the peak shift decay does not reflect the energy transfer process only, the time scales of energy transfer should not be obtained by a multiexponential fit of the peak shift data. However, we can estimate the intra B800 energy transfer time scale by fitting the calculated population decay curve shown in Figure 6b, i.e., the decay of the donor population due to energy transfer *only* within the B800 band. A two-exponential fit of the donor decay curve (Figure 6b) yields two components, a 500−600 fs (±100 fs) component with an amplitude of ∼75% and a ∼2 ps component with an amplitude of ∼25%. Since our model fits the peak shift data reasonably well, we can attribute the 500−600 fs decay component in the data to the ensemble-averaged depopulation time scale of an excitation that is created on a B800 chromophore *only* due to energy transfer within the B800 band. The ∼2 ps component cannot be accurately obtained from the peak shift data as the data was collected until 1.2 ps.

Clearly any correct model must also simulate the linear absorption spectrum. The absorption spectrum of the B800 band has contributions from the vibronic band and the upper excitonic edge of the B850 band. Scholes and Fleming have recently simulated the absorption spectrum of the B850 band in the $Q_y$ region.[16] We subracted the simulated B850 absorption spectrum from the total B800−850 absorption spectrum ($Q_y$ region), and the resultant spectrum is shown in Figure 7 (solid circles). The $M(t)$ that we obtained to simulate the peak shift data is used to simulate the absorption spectrum via the relation

$$\sigma(\omega) \propto \int_{-\infty}^{\infty} dt \exp[-i(\omega - \omega_{eg}) \exp(-g(t)] \qquad (6)$$

where $\omega_{eg}$ is the transition frequency of the system and $g(t)$ is the line-broadening function that is obtained from $M(t)$.[55] The simulated absorption spectrum is shown in Figure 7 as a dashed line. Clearly, the simulated spectrum is much broader than the experimental absorption spectrum of the B800 band. Minor adjustments of the Gaussian time scale and its coupling strength in an $M(t)$ that still reproduces the peak shift data could not generate a satisfactory absorption spectrum. The reason that we cannot reproduce the absorption spectrum is that we have to use a much larger value of static disorder to simulate the peak shift data than is consistent with the absorption spectrum. To correctly simulate the absorption spectrum, the standard deviation of the static disorder distribution should be ∼100 cm$^{-1}$. This, however, cannot correctly reproduce the peak shift data (especially the long-time value of peak shift) with only one level of disorder. A peak shift simulation is shown in Figure 5, curve (iv), with one level of disorder with a width of 100 cm$^{-1}$, and it is clearly not in agreement with the experimental data. It underestimates the experimental peak shift data value, more so at longer time delays. Hence this model cannot simultaneously reproduce both the peak shift data and the absorption spectrum.

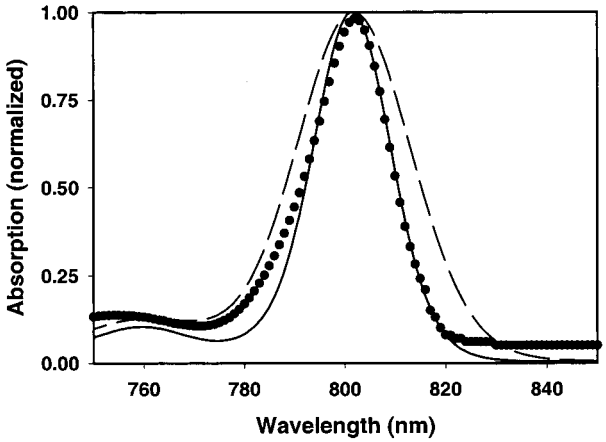


**Figure 7.** B800-only absorption spectrum (solid circles) obtained after removing the contribution from the B850 absorption spectrum. The dashed line shows the simulated B800 absorption spectrum with a disorder width of 150 cm$^{-1}$, and the solid line is the simulated spectrum with a disorder width of 100 cm$^{-1}$.

**Case 2. $\sigma$, $\Sigma \neq 0$ (Partially Correlated Disorder).** A possible explanation for the difficulty in fitting both the absorption spectrum and the peak shift data with a common value of $\sigma$ could be that only a portion of the total inhomogeneous width directly influences in the energy transfer process. This is the case for a nonzero value of $\Sigma$ since the energy transfer process within each LH2 complex averages only over the distribution described by $\sigma$. The $\Sigma$ distribution remains as a contribution to the static disorder of the entire ensemble and thus influences the final value of the peak shift. The absorption spectrum appears to be consistent with a total value of the disorder of $\Delta \sim 100$ cm$^{-1}$, and thus our approach in this section is to apportion this total width to both $\sigma$ and $\Sigma$. Changing $\sigma$ has a relatively minor effect on the population kinetics as Figure 8 shows, but changing $\sigma$ and $\Sigma$ significantly influences the peak shift. In Figure 8 we have shown the population kinetics without the B800−850 energy transfer as we would like to emphasize that the intra-B800 energy transfer dynamics is predominantly responsible for the 500−600 fs peak shift decay. However, all peak shift calculations are done taking into account the B800−850 energy transfer. To calculate the peak shift, population kinetics are determined for the particular $\sigma$ value as described previously and then they are combined with the appropriate response functions as outlined in ref 44. The value of $\Sigma$ does not affect the population kinetics, but it does affect the peak shift.

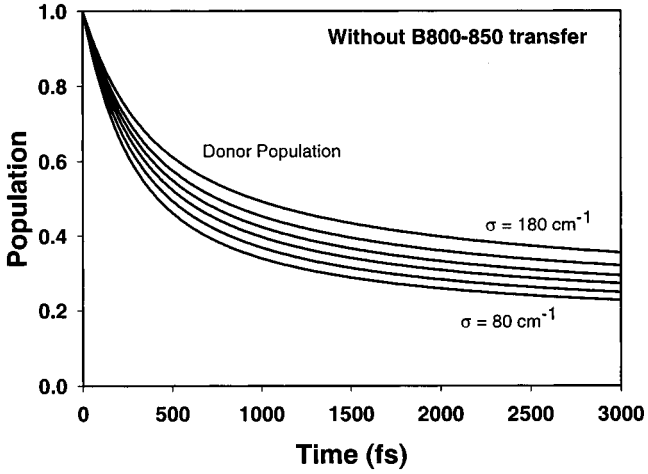


**Figure 8.** Ensemble-averaged donor population kinetics (B800 band) without interband energy transfer to the B850 band for different values of $\sigma$. The effect of varying $\sigma$ can be seen clearly when the B800−850 energy transfer is neglected. From bottom to top $\sigma$ is varied from 80 to 180 $cm^{-1}$ in increments of 20 $cm^{-1}$.

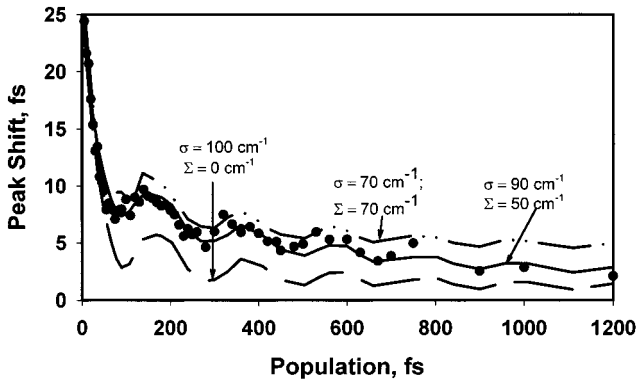


**Figure 9.** Solid circles are the experimental peak shift data. The dashed curve is a simulation for uncorrelated disorder ($\sigma = 100$ $cm^{-1}$, $\Sigma = 0$). The dash−dot−dot and solid curves are for partly correlated disorder: dash−dot−dot ($\sigma = 70$ $cm^{-1}$, $\Sigma = 70$ $cm^{-1}$); solid line ($\sigma = 90$ $cm^{-1}$, $\Sigma = 50$ $cm^{-1}$).

In Figure 9 we show peak shift simulations with different values of $\sigma$ and $\Sigma$ (keeping the total width of the distribution fixed at 100 $cm^{-1}$), and the simulation that best describes the data is for $\sigma = 90$ $cm^{-1}$ and $\Sigma = 50$ $cm^{-1}$. As expected, a nonzero value of $\Sigma$ leads to a finite value of long-time peak shift. The simulated absorption spectrum using $\sigma = 90$ and $\Sigma = 50$ $cm^{-1}$ is shown in Figure 7 (solid line) and fits the spectrum quite well. Thus we now have a consistent description of both the peak shift and the linear absorption spectrum. A two-level-disorder model has been previously introduced by Frieberg et al. to simulate the low-temperature pump−probe difference absorption spectrum of the B800 band.[56] However, the evidence for the presence of two levels of disorder from pump−probe studies is not very compelling. Recently, single molecule spectroscopy at extremely low temperatures has also suggested the presence of two levels of disorder in the B800 band of the LH2 complex of *Rps. acidophila*.[41] Our values of $\sigma = 90$ $cm^{-1}$ and $\Sigma = 50$ $cm^{-1}$ compare quite well with the values obtained from the other spectroscopic techniques.[41,56]

### 6. Discussion and Concluding Remarks

The analysis described here presents several advances over previous studies of energy transfer via the three pulse photon echo peak shift. The first such study also involved the B800 band of LH2 in a different species, *Rb. sphaeroides*,[43] and the peak shift decay curve was very similar to the one obtained for *Rps. acidophila*. The peak shift for *Rb. sphaeroides* was also found to decay on a time scale of ∼600 fs to a value of ∼2−3 fs on a 2 ps population period. The peak shift *did not* decay to zero on a 2 ps time scale. This work ascribed the 500−600 fs decay to B800−B850 energy transfer, rather than to B800−B800 energy transfer. The data were analyzed using a simple two-level model, and the energy transfer component was modeled as an exponential term in $M(t)$. While in the initial study the insensitivity to simple population decay was appreciated, the influence of a distribution of site energies was not.

The formalism used here allows us to significantly improve on the level of microscopic detail used to describe the peak shift compared to our study of the plant light-harvesting complex LHCII.[39] In particular we do not require phenomenological rate constants as input parameters and the contributions of reversible energy transfer and a distribution of rates resulting from energy disorder can be properly included in the model. With such a microscopic model including electron−phonon coupling, static disorder, and electronic coupling, our results show that Forster transfer provides an accurate description of energy migration within the weakly coupled, essentially monomeric B800 chromophores of LH2. The ensemble-averaged calculations reproduce the 100 fs−1.2 ps time range of the peak shift data very well, and we therefore conclude that the 500−600 fs decay component in the peak shift reflects B800−B800 energy transfer.

Using a simple model of disorder, we were unable to provide a satisfactory description of both the peak shift and the absorption spectrum. The introduction of two levels of disorder, i.e., a simple model for correlated disorder, allows us to simulate both pieces of data with a common set of parameters. It is interesting to note that, in the previous study of peak shift of the B800 band of *Rb. sphaeroides* by Joo et al.,[43] the amplitude of the energy transfer component (modeled as an exponential decay in $M(t)$) was estimated to be ∼90 $cm^{-1}$ and the disorder was estimated to be ∼50 $cm^{-1}$. The 50 $cm^{-1}$ disorder value reproduced the ∼2−3 ps peak shift value at long times (2 ps). We have used a more sophisticated model of energy transfer and disorder in this paper and have estimated the intracomplex inhomogeneity to be ∼90 $cm^{-1}$ and the intercomplex inhomogeneity to be ∼50 $cm^{-1}$. These values are exactly the same as reported by Joo et al., which suggests that by using a simplified model for peak shift for weakly coupled energy transfer systems reasonable estimates of energy transfer time scales and disorder can be made; however, the conclusions can differ. The apparent success of our model with a relatively small distribution of means ($\Sigma = 50$ $cm^{-1}$) compared to the energy level distributions within a single complex ($\sigma = 90$ $cm^{-1}$) suggests that the energy transfer dynamics are dominated by local disorder. This disorder may result from a variety of effects such as side chain orientations, distortions from planarity of individual B800 molecules, contributions from ionized and neutral groups close to their p*K*, and specific hydrogen bond interactions. Global distortions of individual complexes arising from, e.g., distortions from circular symmetry,[57] variations in the number of $\alpha$, $\beta$ pairs per complex, or binding of ions, could lead to shifts of transition frequency of a significant fraction of the B800 molecules in a particular complex, and thus a nonzero value of $\Sigma$. A more sophisticated model would likely include a correlation length that takes into account the spatial distribution of the energetic disorder. However, until more is known about the specific molecular origins of energy disorder, development of such a model does not seem justified.

Finally, we note the success of the 3PEPS technique in a system where the experimental time window is severely limited as a result of interband energy transfer. We hope that the approach described here will facilitate analysis of complex energy transfer systems in a variety of contexts.

**Note Added in Proof.** In addition to the types of global distortion described in the text, the mean energy of a complex can arise from incomplete statistical sampling. Since the number of BChl molecules in an LH2 complex is too small to achieve a well-behaved distribution, a portion of $\Sigma$ should be attributed to this statistical effect.[58]

**Acknowledgment.** This work was supported by the Director, Office of Science, Office of Basic Energy Sciences, Chemical Sciences Division, of the U.S. Department of Energy under Contract No. DE-AC03-76SF0098. We thank Prof. Richard Cogdell for providing us the samples.

## References and Notes

(1) van Grondelle, R.; Dekker, J. P.; Gillbro, T.; Sundström, V. *Biochim. Biophys. Acta* **1994**, *1187*, 1−65.

(2) McDermott, G.; Prince, S. M.; Freer, A. A.; Hawthornthwaite-Lawless, A. M.; Papiz, M. Z.; Cogdell, R. J.; Isaacs, N. W. *Nature* **1995**, *374*, 517−521.

(3) Koepke, J.; Hu, X.; Muenke, C.; Schulten, K.; Michel, H. *Structure* **1996**, *4*, 581−597.

(4) van Grondelle, R.; Kramer, H. J. M.; Rijgersberg, C. P. *Biochim. Biophys. Acta* **1982**, *682*, 208−215.

(5) van Grondelle, R.; Bergström, H.; Sundström, V.; Gillbro, T. *Biochim. Biophys. Acta* **1987**, *894*, 313.

(6) Sundström, V.; Pullerits, T.; van Grondelle, R. *J. Phys. Chem. B* **1999**, *103*, 2327−2346.

(7) Shreve, A. P.; Trautman, J. K.; Frank, H. A.; Owens, T. G.; Albrecht, A. C. *Biochim. Biophys. Acta* **1991**, *1058*, 280−288.

(8) Hess, S.; Feldchtein, F.; Rabin, A.; Nurgaleev, I.; Pullerits, T.; Sergeev, A.; Sundström, V. *Chem. Phys. Lett.* **1993**, *216*, 247−257.

(9) Hess, S.; Åkesson, E.; Cogdell, R. J.; Pullerits, T.; Sundström, V. *Biophys. J.* **1995**, *69*, 2211−2225.

(10) Pullerits, T.; Hess, S.; Herek, J. L.; Sundström, V. *J. Phys. Chem. B* **1997**, *101*, 10560−10567.

(11) Jimenez, R.; Dikshit, S. N.; Bradforth, S. E.; Fleming, G. R. *J. Phys. Chem.* **1996**, *100*, 6825−6834.

(12) Ma, Y.-Z.; Cogdell, R. J.; Gillbro, T. *J. Phys. Chem. B* **1997**, *101*, 1087.

(13) Ma, Y.-Z.; Cogdell, R. J.; Gillbro, T. *J. Phys. Chem. B* **1998**, *102*, 881.

(14) Kennis, J. T. M.; Streltsov, A. M.; Permentier, H.; Aartsma, T. J.; Amesz, J. *J. Phys. Chem. B* **1997**, *101*, 8369−8374.

(15) Monshouwer, R.; Ortiz de Zarate, I.; van Mourik, F.; van Grondelle, R. *Chem. Phys. Lett.* **1995**, *246*, 341−346.

(16) Scholes, G. D.; Fleming, G. R. *J. Phys. Chem. B* **2000**, *104*, 1854−1868.

(17) Sauer, K.; Cogdell, R. J.; Prince, S. M.; Freer, A.; Isaacs, N. W.; Scheer, H. *Photochem. Photobiol.* **1996**, *64*, 564−576.

(18) Krueger, B. P.; Scholes, G. D.; Fleming, G. R. *J. Phys. Chem. B* **1998**, *102*, 5378−5386.

(19) Kühn, O.; Sundström, V. *J. Chem. Phys.* **1997**, *107*, 4154−4164.

(20) Kuhn, O.; Renger, T.; Voigt, J.; Sundstrom, V. *Trends Photochem. Photobiol.* **1997**, *4*, 213−256.

(21) Jimenez, R.; van Mourik, F.; Yu, J. Y.; Fleming, G. R. *J. Phys. Chem. B* **1997**, *101*, 7350−7359.

(22) Monshouwer, R.; Abrahamsson, M.; van Mourik, F.; van Grondelle, R. *J. Phys. Chem. B* **1997**, *101*, 7241−7248.

(23) Chachisvilis, M.; Kühn, O.; Pullerits, T.; Sundström, V. *J. Phys. Chem. B* **1997**, *101*, 7275−7283.

(24) Leegwater, J. A. *J. Phys. Chem. B* **1996**, *100*, 14403.

(25) Meier, T.; Chernyak, V.; Mukamel, S. *J. Phys. Chem. B* **1997**, *101*, 7332.

(26) Jean, J. M.; Friesner, R. A.; Fleming, G. R. *J. Chem. Phys.* **1992**, *96*, 5827−5842.

(27) Förster, T. Delocalized Excitation and Excitation Transfer. In *Modern Quantum Chemistry*; Sinanoglu, O., Ed.; Academic Press: New York, 1965; Vol. III, pp 93−137.

(28) Kramer, H. J. M.; van Grondelle, R.; Hunter, C. N.; Westerhuis, W. H. J.; Amesz, J. *Biochim. Biophys. Acta* **1984**, *765*, 156−165.

(29) Wu, H.-M.; Savikhin, S.; Reddy, N. R. S.; Jankowiak, R.; Cogdell, R. J.; Struve, W. S.; Small, G. J. *J. Phys. Chem.* **1996**, *100*, 1087.

(30) Wu, H.-M.; Ratsep, M.; Jankowiak, R.; Cogdell, R. J.; Small, G. J. *J. Phys. Chem. B* **1997**, *101*, 7641.

(31) Monshouwer, R.; van Grondelle, R. *Biochim. Biophys. Acta* **1996**, *1275*, 70−75.

(32) De Caro, C.; Visschers, R. W.; van Grondelle, R.; Völker, S. J. *J. Phys. Chem.* **1994**, *98*, 10584−10590.

(33) Joo, T.; Jia, Y.; Yu, J.-Y.; Lang, M. J.; Fleming, G. R. *J. Chem. Phys.* **1996**, *104*, 1.

(34) Cho, M.; Yu, J.-Y.; Joo, T.; Nagasawa, Y.; Passino, S. A.; Fleming, G. R. *J. Phys. Chem.* **1996**, *100*, 11944.

(35) Fleming, G. R.; Cho, M. *Annu. Rev. Phys. Chem.* **1996**, *47*, 109−134.

(36) Yu, J.-Y.; Nagasawa, Y.; van Grondelle, R.; Fleming, G. R. *Chem. Phys. Lett.* **1997**, *280*, 404−410.

(37) Groot, M.-L.; Yu, J.-Y.; Agarwal, R.; Norris, J. R.; Fleming, G. R. *J. Phys. Chem. B* **1998**, *102*, 5923−5931.

(38) Yang, M.; Fleming, G. R. *J. Chem. Phys.* **1999**, *111*, 27.

(39) Agarwal, R.; Krueger, B.; Scholes, G. D.; Yang, M.; Yom, J.; Mets, L.; Fleming, G. R. *J. Phys. Chem. B* **2000**, *104*, 2908−2918.

(40) Jean, J. M.; Chan, C.-K.; Fleming, G. R. *Isr. J. Chem.* **1988**, *28*, 169−175.

(41) van Oijen, A. M.; Ketelaars, M.; Kohler, J.; Aartsma, T. J.; Schmidt, J. *Biophys. J.* **2000**, *78*, 1570−1577.

(42) Passino, S. A.; Yutaka, N.; Joo, T.; Fleming, G. R. *J. Phys. Chem. A* **1997**, *101*, 725−731.

(43) Joo, T.; Jia, Y.; Yu, J.-Y.; Jonas, D. M.; Fleming, G. R. *J. Phys. Chem.* **1996**, *100*, 2399−2409.

(44) Yang, M.; Fleming, G. R. *J. Chem. Phys.* **2000**, *113*, 2823.

(45) Nagasawa, Y.; Passino, S. A.; Joo, T.; Fleming, G. R. *J. Chem. Phys.* **1997**, *106*, 4840−4852.

(46) Nagasawa, Y.; Yu, J.-Y.; Cho, M.; Fleming, G. R. *Faraday Discuss.* **1997**, *108*, 23−34.

(47) Reddy, N. R. S.; Small, G. J.; Seibert, M.; Picorel, R. *Chem. Phys. Lett.* **1991**, *181*, 391.

(48) Pullerits, T.; van Mourik, F.; Monshouwer, R.; Visschers, R. W.; van Grondelle, R. *J. Lumin.* **1994**, *58*, 168.

(49) Ohta, K.; Larsen, D. S.; Yang, M.; Fleming, G. R. Submitted for publication in *J. Chem. Phys.*

(50) Kumble, R.; Palese, S.; Visschers, R. W.; Dutton, P. L.; Hochstrasser, R. M. *Chem. Phys. Lett.* **1996**, *261*, 396.

(51) Visschers, R. W.; Chang, M. C.; van Mourik, F.; Parkesloach, P. S.; Heller, B. A.; Loach, P. A.; Vangrondelle, R. *Biochemistry* **1991**, *30*, 5734−5742.

(52) van Oijen, A. M.; Ketelaars, M.; Kohler, J.; Aartsma, T. J.; Schmidt, J. *J. Phys. Chem. B* **1998**, *102*, 9363−9366.

(53) van Oijen, A. M.; Ketelaars, M.; Kohler, J.; Aartsma, T. J.; Schmidt, J. *Chem. Phys.* **1999**, *247*, 53−60.

(54) Tietz, C.; Chekhlov, O.; Drabenstedt, A.; Wrachtrup, J. *J. Phys. Chem. B* **1999**, *103*, 6328−6333.

(55) Mukamel, S. *Principles of Nonlinear Optical Spectroscopy*; Oxford University Press: New York, 1995.

(56) Frieberg, A.; Timpmann, K.; Ruus, R.; Woodbury, N. W. *J. Phys. Chem. B* **1999**, *103*, 10032−10041.

(57) van Oijen, A. M.; Ketelaars, M.; Kohler, J.; Aartsma, T. J.; Schmidt, J. *Science* **1999**, *285*, 400.

(58) Yang, M.; Agarwal, R.; Fleming, G. R. Submitted for publication in *J. Photochem. Photobiol. A* Lord Porter Issue.